Dynamics of Stripe Patterns in Supersolid Spin-Orbit-Coupled Bose Gases

Kevin T. Geier,[1,2,3,*] Giovanni I. Martone,[4,5,6,†] Philipp Hauke,[1,2] Wolfgang Ketterle,[7,8] and Sandro Stringari[1,2]

[1]*Pitaevskii BEC Center, CNR-INO and Dipartimento di Fisica, Università di Trento, 38123 Trento, Italy*
[2]*Trento Institute for Fundamental Physics and Applications, INFN, 38123 Trento, Italy*
[3]*Institute for Theoretical Physics, Ruprecht-Karls-Universität Heidelberg, Philosophenweg 16, 69120 Heidelberg, Germany*
[4]*Laboratoire Kastler Brossel, Sorbonne Université, CNRS, ENS-PSL Research University, Collège de France, 4 Place Jussieu, 75005 Paris, France*
[5]*CNR NANOTEC, Institute of Nanotechnology, Via Monteroni, 73100 Lecce, Italy*
[6]*INFN, Sezione di Lecce, 73100 Lecce, Italy*
[7]*MIT-Harvard Center for Ultracold Atoms, Cambridge, Massachusetts 02138, USA*
[8]*Department of Physics, Massachusetts Institute of Technology, Cambridge, Massachusetts 02139, USA*

(Received 19 October 2022; revised 17 January 2023; accepted 28 February 2023; published 12 April 2023)

Despite ground-breaking observations of supersolidity in spin-orbit-coupled Bose-Einstein condensates, until now the dynamics of the emerging spatially periodic density modulations has been vastly unexplored. Here, we demonstrate the nonrigidity of the density stripes in such a supersolid condensate and explore their dynamic behavior subject to spin perturbations. We show both analytically in infinite systems and numerically in the presence of a harmonic trap how spin waves affect the supersolid's density profile in the form of crystal waves, inducing oscillations of the periodicity as well as the orientation of the fringes. Both these features are well within reach of present-day experiments. Our results show that this system is a paradigmatic supersolid, featuring superfluidity in conjunction with a fully dynamic crystalline structure.

DOI: 10.1103/PhysRevLett.130.156001

Supersolidity is an intriguing phenomenon exhibited by many-body systems, where both superfluid and crystalline properties coexist as a consequence of the simultaneous breaking of phase symmetry and translational invariance [1–6]. After unsuccessful attempts in solid helium [7,8], supersolidity was first experimentally realized in Bose-Einstein condensates (BECs) with spin-orbit coupling (SOC) [9,10] or inside optical resonators [11]. More recently, the supersolid phase has been identified in a series of experiments with dipolar Bose gases, where phase coherence, spatial modulations of the density profile, as well as the Goldstone modes associated with the superfluid and crystal behavior have been observed [12–19].

Since the experimental realization of spin-orbit-coupled Bose-Einstein condensates (SOC BECs) [20,21], this platform has emerged as a peculiar candidate of supersolidity because the spin degree of freedom is coupled to the density of the system [22–29]. Without SOC, a two-component BEC has already two broken symmetries, one for the absolute phase and one for the relative phase between the two BEC order parameters. The addition of weak SOC mixes the spatial and spin degree of freedom, resulting in a stripe phase where the relative phase between the two condensates breaks the translational symmetry of space—the defining property of a supersolid. The Goldstone modes associated with the relative phase are spin excitations, whose dispersion relations as a function of the Raman coupling have been explored in Refs. [28,30], but a connection to the crystal dynamics of the stripes has so far only been established for their rigid zero-frequency translational motion [28,29].

The rigidity of the stripe pattern has been controversially discussed in the literature. For supersolids induced by coupling a BEC to two single-mode cavities [11,31], the wave vector of the density modulations is determined by the cavity light and the associated Goldstone mode is suppressed for nonzero wave vectors [32]. Since the spin-orbit effect is induced by Raman laser beams, it has been widely believed that the stripe pattern in SOC BECs is also externally imposed by the light and thus rigid. Up to now, conclusive evidence for the nonrigidity of the stripe pattern has been lacking, as previous studies of stripe dynamics have mainly focused on the infinite-wavelength limit [28,29]. In this Letter, we elucidate the lattice-phonon nature of the spin Goldstone mode at finite wavelengths and thus demonstrate that the stripes form a fully dynamic crystal that is by no means rigid. Specifically, we show how spin perturbations can excite oscillations of both the spacing and the orientation of the density fringes, establishing SOC BECs as paradigm examples of supersolidity.

Origin of stripe dynamics.—We consider the common scenario where SOC is generated in a binary mixture of atomic quantum gases by coupling two internal states using a pair of intersecting Raman lasers [34–36]. In contrast to quantum mixtures with a simple coherent coupling of radio frequency or microwave type, the Raman coupling involves

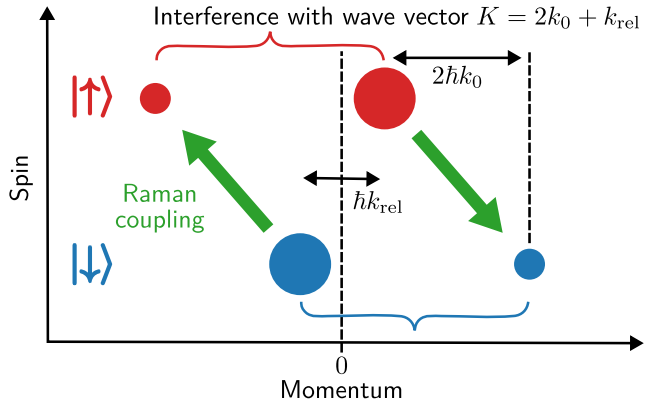

FIG. 1. Illustration of the interference effects that lead to the appearance and dynamics of stripe patterns. The Raman process responsible for spin-orbit coupling turns the two-component Bose-Einstein condensate (two big circles) into a system with a four-component wave function. Components with the same spin form a spatial interference pattern.

a finite momentum transfer $-2\hbar\boldsymbol{k}_0 = -2\hbar k_0\hat{\boldsymbol{e}}_x$, which we assume to point in the negative x direction. In the limit of weak Raman coupling, the emergence of the stripes and their dynamics can simply be explained as a spatial interference effect within a wave function which has four components (Fig. 1): spin-up condensate at zero momentum with a SOC admixture of spin down at wave vector $2\boldsymbol{k}_0$, and spin-down condensate at zero momentum with a SOC admixture of spin up at wave vector $-2\boldsymbol{k}_0$. Because of SOC, there is now a spatial interference pattern between the two spin-up and two spin-down components with wave vector $\boldsymbol{K} = 2\boldsymbol{k}_0$. The spontaneously chosen relative phase between the two condensates determines the origin of the stripe pattern. If there is a chemical potential difference between the two components, the relative phase of the two condensates will oscillate and therefore also the position of the stripes. One can add a spin current to the system, e.g., an out-of-phase or relative motion between the two condensates, which thus obtain the momenta $\pm\hbar\boldsymbol{k}_{\rm rel}/2$. The four components of the wave function are now at $\boldsymbol{k}_{\rm rel}/2$, $-\boldsymbol{k}_{\rm rel}/2 - 2\boldsymbol{k}_0$ for spin up and $-\boldsymbol{k}_{\rm rel}/2, \boldsymbol{k}_{\rm rel}/2 + 2\boldsymbol{k}_0$ for spin down, and the spatial interference pattern has now the wave vector $\boldsymbol{K} = 2\boldsymbol{k}_0 + \boldsymbol{k}_{\rm rel}$. If the spin current is oscillating, the wave vector of the stripe pattern will oscillate at the same frequency. When $\boldsymbol{k}_{\rm rel}$ is parallel to $\boldsymbol{k}_0$, the fringe spacing oscillates. When they are perpendicular, the angle of the fringes oscillates. In what follows, we confirm and extend this intuitive picture using rigorous perturbative calculations and numerical simulations.

Theoretical framework.—After transforming to a spin-rotated frame, the single-particle Hamiltonian of the system takes the time-independent form [21]

$$H_{\rm SOC} = \frac{1}{2m}(\boldsymbol{p} - \hbar\boldsymbol{k}_0\sigma_z)^2 + \frac{\hbar\Omega}{2}\sigma_x + \frac{\hbar\delta}{2}\sigma_z + V(\boldsymbol{r}), \qquad (1)$$

where m is the atomic mass, σ_x and σ_z are Pauli matrices, Ω is the strength of the Raman coupling, δ is the effective detuning, and $V(\boldsymbol{r})$ is a single-particle potential. In infinite systems ($V \equiv 0$), the Hamiltonian is translationally invariant and allows for a spontaneous breaking of this symmetry, which, in combination with the broken $U(1)$ symmetry in the BEC phase, gives rise to supersolidity.

Since quantum depletion of a SOC BEC is typically small under realistic conditions [37,38], interactions between atoms are well described by mean-field theory via the Gross-Pitaevskii (GP) energy functional [39]

$$E = \int \mathrm{d}\boldsymbol{r}\left(\Psi^\dagger H_{\rm SOC}\Psi + \frac{g_{nn}}{2}n^2 + \frac{g_{ss}}{2}s_z^2 + g_{ns}ns_z\right). \qquad (2)$$

Here, the order parameter is given by a two-component spinor $\Psi = (\Psi_\uparrow, \Psi_\downarrow)^\intercal$ with complex wave functions $\Psi_\uparrow$ and $\Psi_\downarrow$ for the individual spin states. The last three terms in Eq. (2) describe density-density, spin-spin, and density-spin interactions, respectively, where $n = |\Psi_\uparrow|^2 + |\Psi_\downarrow|^2$ denotes the total particle density and $s_z = |\Psi_\uparrow|^2 - |\Psi_\downarrow|^2$ is the spin density. The corresponding interaction constants $g_{nn} = (g_{\uparrow\uparrow} + g_{\downarrow\downarrow} + 2g_{\uparrow\downarrow})/4$, $g_{ss} = (g_{\uparrow\uparrow} + g_{\downarrow\downarrow} - 2g_{\uparrow\downarrow})/4$, and $g_{ns} = (g_{\uparrow\uparrow} - g_{\downarrow\downarrow})/4$ are obtained from suitable combinations of the coupling constants $g_{ij} = 4\pi\hbar^2 a_{ij}/m$, determined by the s-wave scattering lengths a_{ij} of the respective spin channels with $i, j \in \{\uparrow, \downarrow\}$. We focus our analysis on symmetric intraspecies interactions, assuming $g_{ns} = 0$ and $\delta = 0$ from now on.

At the critical Raman coupling $\hbar\Omega_{\rm cr} = 4E_r\sqrt{2g_{ss}/(g_{nn} + 2g_{ss})}$ [23,25], where $E_r = (\hbar k_0)^2/2m$ is the recoil energy, the system undergoes a first-order transition between the supersolid (stripe) phase and the superfluid (but not supersolid) so-called plane-wave and single-minimum phases (see, e.g., Ref. [27]). The latter are characterized by a strong Raman coupling that is responsible for the locking of the relative phase between the two spin components [40], resulting from the competition between the spin (g_{ss}) and density (g_{nn}) interaction components of the mean-field energy functional (2) [41]. Consequently, there is only a single spin-density-hybridized Goldstone mode above $\Omega_{\rm cr}$. Conversely, in the supersolid phase, below $\Omega_{\rm cr}$, the spontaneous breaking of both phase and translational symmetry implies the existence of two Goldstone modes of predominantly density and spin nature with distinct sound velocities (see Supplemental Material [42] for further details) [26,29].

A major question to be addressed in what follows is how the spin degree of freedom can induce dynamics in the stripe patterns and in particular how the excitation of a spin wave results in the excitation of a crystal wave affecting the time dependence of the density profile.

Perturbation approach in infinite systems.—A useful scenario to probe this question consists in suddenly

releasing at time $t = 0$ a small static spin perturbation of the form $-\lambda E_r \sigma_z \cos(\boldsymbol{q}\cdot\boldsymbol{r})$, with $0 < \lambda \ll 1$. The wave vector $\boldsymbol{q}$ is assumed to be small in order to explore the relevant phonon regime, where a major effect of the release of the perturbation is the creation of a spin wave propagating with velocity c_s. Here, we are mainly interested in its effect on the dynamic behavior of the stripes characterizing the density distribution. Starting from the results of Ref. [29] for the Bogoliubov amplitudes of the phonon modes in the long-wavelength limit, and neglecting the small contributions of the gapped modes of the Bogoliubov spectrum, the space and time dependence of the density can be written in the form

$$n(\boldsymbol{r},t) = \bar{n} + \sum_{\bar{m}=1}^{+\infty} \tilde{n}_{\bar{m}} \cos[\bar{m}\chi(\boldsymbol{r},t)]. \tag{3}$$

Here, $\bar{n}$ is the average density and

$$\chi(\boldsymbol{r},t) = 2k_1 x + \phi + \delta\phi(t)\cos(\boldsymbol{q}\cdot\boldsymbol{r}) \tag{4}$$

the relative phase between the two condensates in the spin-rotated frame. The sum over the integer index $\bar{m}$ reflects the presence of higher harmonics in the density profile (3) characterizing the stripe phase, whose coefficients are denoted by $\tilde{n}_{\bar{m}}$. Equations (3) and (4) explicitly reveal that the perturbed density fringes are a combined effect of the equilibrium modulations, fixed by the wave vector $2\boldsymbol{k}_1 = 2k_1\hat{\boldsymbol{e}}_x$ (which differs from $2\boldsymbol{k}_0$ at finite Raman coupling [25,29]), and those induced by the external perturbation, characterized by the wave vector $\boldsymbol{q}$. The perturbative expression for k_1 is reported in Ref. [29] and for convenience in the Supplemental Material [42]. The phase ϕ represents the spontaneously chosen offset of the stripe pattern in equilibrium. The time dependence of the function $\delta\phi$ is fixed by the sound velocities $c_{n,s}$ of the density and spin phonons as well as by the Raman coupling Ω.

For $q \ll k_1$, the relative phase (4) varies very slowly over a large number of equilibrium density oscillations. Consequently, in a region of space $|\boldsymbol{r}-\boldsymbol{r}_0| \ll q^{-1}$ around a given point $\boldsymbol{r}_0$, one can approximate χ by its first-order Taylor expansion,

$$\chi(\boldsymbol{r},t) \simeq \boldsymbol{K}(\boldsymbol{r}_0,t)\cdot\boldsymbol{r} + \Phi(\boldsymbol{r}_0,t). \tag{5}$$

This expression features a local time-dependent stripe wave vector, whose structure

$$\boldsymbol{K}(\boldsymbol{r}_0,t) = \nabla\chi(\boldsymbol{r}_0,t) = 2\boldsymbol{k}_1 - \delta\phi(t)\sin(\boldsymbol{q}\cdot\boldsymbol{r}_0)\boldsymbol{q} \tag{6}$$

confirms the intuitive scenario of Fig. 1 (where $\boldsymbol{k}_1$ has been approximated by $\boldsymbol{k}_0$), upon identifying $\boldsymbol{k}_{\rm rel}$ with the second term in Eq. (6). In addition, Eq. (5) contains the phase shift

$$\begin{aligned}\Phi(\boldsymbol{r}_0,t) &= \chi(\boldsymbol{r}_0,t) - \boldsymbol{r}_0\cdot\nabla\chi(\boldsymbol{r}_0,t)\\ &= \phi + \delta\phi(t)[\cos(\boldsymbol{q}\cdot\boldsymbol{r}_0) + (\boldsymbol{q}\cdot\boldsymbol{r}_0)\sin(\boldsymbol{q}\cdot\boldsymbol{r}_0)],\end{aligned} \tag{7}$$

which is responsible for the time modulation of the offset of the stripe pattern.

Carrying out a perturbative analysis of the order parameter of the condensate up to second order in $\hbar\Omega/4E_r$ (see Refs. [29,44]) yields the result

$$\delta\phi(t) = -\frac{2k_1 v_s}{c_s q}\sin(c_s q t), \tag{8}$$

where we have introduced the velocity

$$v_s = \lambda\frac{\hbar k_0}{m}\left[\frac{1}{2} - \beta\left(\frac{\hbar\Omega}{4E_r}\right)^2\right], \tag{9}$$

with $\beta = E_r\bar{n}[2E_r g_{nn} + 2(2E_r + \bar{n}g_{nn})g_{ss} + \bar{n}g_{ss}^2]/[2(2E_r + \bar{n}g_{nn})^2(2E_r + \bar{n}g_{ss})]$, and the expression for c_s is reported in Ref. [29] and for convenience in the Supplemental Material [42]. At the leading order Ω^2, only the spin sound velocity c_s enters Eq. (8), while a second term oscillating at the density phonon frequency $c_n q$ appears at order Ω^4 [44]. For $\Omega = 0$, the velocity v_s fixes the time variation rate of the relative phase of the quantum mixture, without any consequence for the density distribution since the contrast of fringes exactly vanishes in this limit [25,29] (see also Supplemental Material [42]).

If $\cos(\boldsymbol{q}\cdot\boldsymbol{r}_0) = \pm 1$, the initial static spin perturbation has a peak (antinode) at $\boldsymbol{r}_0$, and close to this point it becomes of the form $\mp\lambda E_r\sigma_z$. After releasing the spin perturbation, there is a spin imbalance at $\boldsymbol{r}_0$ and the difference in chemical potentials causes an oscillation of the relative phase of the two condensates. From Eqs. (7) and (8) one sees that, at times satisfying the condition $t \ll (c_s q)^{-1}$ (which is easily fulfilled for the small q of interest here), the stripes show a displacement at velocity $\pm v_s$, i.e., $\chi(\boldsymbol{r},t) \simeq 2k_1(x \mp v_s t) + \phi$, in excellent agreement with the numerical findings of Ref. [28] (see Supplemental Material [42] for further details). At $q = 0$, the spatial translation of stripes corresponds to the zero-frequency limit of the spin Goldstone branch.

Far from the antinodes, after the spin quench there is an oscillating spin current, which makes also the stripe wave vector (6) vary in time. The strongest oscillations occur when $\sin(\boldsymbol{q}\cdot\boldsymbol{r}_0) = \pm 1$, i.e., $\boldsymbol{r}_0$ is a node of the initial perturbation, which is thus antisymmetric under inversion with respect to $\boldsymbol{r}_0$ and locally behaves as $\pm\lambda E_r\boldsymbol{q}\cdot(\boldsymbol{r}-\boldsymbol{r}_0)\sigma_z$. In particular, if $\boldsymbol{q} = q\hat{\boldsymbol{e}}_x$, the local stripe wavelength $2\pi/|\boldsymbol{K}(\boldsymbol{r}_0,t)| = [1 \mp (v_s/c_s)\sin(c_s q t)]\pi/k_1$ oscillates around its equilibrium value. By contrast, if $\boldsymbol{q} = q\hat{\boldsymbol{e}}_y$, the stripes rotate by an angle $\pm(v_s/c_s)\sin(c_s q t)$ about the z axis. This effect occurs in combination with the fringe displacement seen above, unless $\boldsymbol{r}_0$ coincides with a maximum or minimum of the equilibrium density distribution.

The above discussion shows that a spin perturbation applied to the stripe configuration can cause a rigid motion

of the stripes as well as a periodic change in either magnitude or orientation of their wave vector, depending on the local behavior of the perturbation. Although the analytic results (8) and (9) have been derived by carrying out a perturbative analysis up to order Ω^2, we have verified that they provide a rather accurate description of the dynamics of stripes, as compared to a numerical solution of the time-dependent linearized GP equation in infinite systems, also for fairly large values of the Raman coupling.

Numerical simulations in a harmonic trap.—Having understood how spin perturbations affect the dynamics of the stripe pattern in infinite systems, we now illustrate similar effects taking place in finite-size configurations, namely, in the presence of a harmonic trapping potential $V(\boldsymbol{r}) = m(\omega_x^2 x^2 + \omega_y^2 y^2 + \omega_z^2 z^2)/2$ with angular frequencies ω_i and corresponding oscillator lengths $a_i = \sqrt{\hbar/m\omega_i}$, $i = x, y, z$. To this end, we numerically solve the full time-dependent GP equations, which can be derived by applying the variational principle $i\hbar\partial_t \Psi_{\uparrow/\downarrow} = \delta E/\delta \Psi^*_{\uparrow/\downarrow}$ to the energy functional (2).

For our numerics, we assume symmetric intraspecies scattering lengths close to those of ^{87}Rb, where the majority of experiments on SOC BECs has been conducted, $a_{\uparrow\uparrow} = a_{\downarrow\downarrow} = 100a_0$ (a_0 is the Bohr radius). Moreover, to enhance the miscibility of the two spin species and thus the supersolid features, we assume a quasi-two-dimensional (2D) situation with reduced interspecies coupling $\tilde{g}_{\uparrow\downarrow} = 0.6\tilde{g}_{\uparrow\uparrow}$ (see experimental considerations below), where $\tilde{g}_{\uparrow\uparrow} = \tilde{g}_{\downarrow\downarrow} = g_{\uparrow\uparrow}/\sqrt{2\pi}a_z$ are effective 2D couplings for a strong vertical confinement with frequency $\omega_z/2\pi = 2500$ Hz [45]. Further, we choose an elongated trap in the x direction with $(\omega_x, \omega_y) = 2\pi(50, 200)$ Hz, a total particle number of $N = 10^4$, as well as $k_0 = \sqrt{2}\pi/\lambda_0$ with $\lambda_0 = 804.1$ nm [21].

The numerical protocol is the same as that in the quench scenario considered above: we first compute the ground state in the presence of a small static perturbation of spin nature and then observe the dynamics after suddenly releasing the perturbation at time $t = 0$. Here, our analysis is focused on the stripe dynamics generated by the longitudinal and transversal spin operators $x\sigma_z$ and $y\sigma_z$, which correspond in infinite systems to the local behavior of the perturbation around the nodes. The translational motion of the stripes induced by the uniform spin operator σ_z, corresponding to a sudden change of the Raman detuning, has been studied numerically in Ref. [28] and is further detailed in the Supplemental Material [42].

Figures 2(a) and 2(b) illustrate, respectively, the oscillation of the fringe spacing and the periodic rotation of the stripe wave vector in response to weak perturbations by the operators $x\sigma_z$ and $y\sigma_z$. The corresponding oscillation frequencies coincide with those of the induced spin-dipole oscillations $\langle x\sigma_z\rangle$ and $\langle y\sigma_z\rangle$, as shown in Figs. 2(c) and 2(d), respectively. It is remarkable that the transversal spin

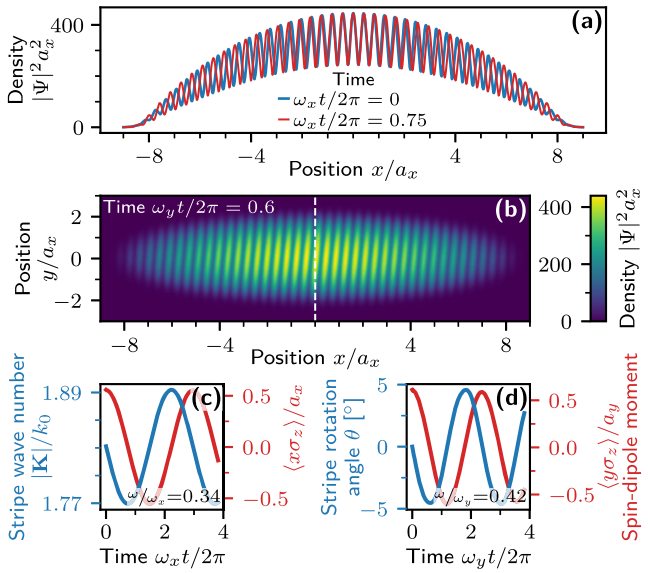

FIG. 2. Dynamics of the stripe pattern in a harmonically trapped system for $\hbar\Omega/E_r = 1.75$. (a),(b) Snapshots of the density profile at different times, showing the compression and dilatation of the fringe spacing (a) as well as the rotation of the stripes (b) after suddenly releasing the longitudinal and transversal spin perturbations $H_{x\sigma_z} = -m\omega_x^2 x_0\, x\sigma_z$ with $x_0/a_x = 0.1$ and $H_{y\sigma_z} = -m\omega_y^2 y_0\, y\sigma_z$ with $y_0/a_y = 0.15$, respectively. (c) Evolution of the magnitude of the stripe wave vector $|\boldsymbol{K}|$ and of the longitudinal spin-dipole moment $\langle x\sigma_z\rangle$ for the scenario in (a). (d) Time trace of the rotation angle θ of the stripes and of the transversal spin-dipole moment $\langle y\sigma_z\rangle$ for the scenario in (b). The oscillation frequencies of the stripe pattern coincide with those of the corresponding spin-dipole moments.

operator $y\sigma_z$, which generates the oscillating rotation of the stripes in the supersolid phase, also constitutes a crucial spin contribution to the angular momentum operator as a consequence of SOC [46,47]. The inclusion of such an effective y-dependent detuning has been used to generate quantized vortices [20] and to show the occurrence of crucial rigid components in the moment of inertia [48].

Unsurprisingly, owing to nonlinear effects in the SOC strength, the dynamic excitation of stripes is not only produced by spin perturbations (as considered above), but also by density perturbations. A density perturbation mainly excites the associated density Goldstone mode, but due to SOC also produces a weak cross excitation of the spin Goldstone mode. Since the density mode also has a weak manifestation in the spin sector, quantities sensitive to the spin degree of freedom, e.g., the fringes, exhibit a beat note involving the frequencies of both Goldstone modes [49]. In fact, one can show that a density perturbation generates a beating oscillation of the stripe wave vector with an amplitude of order Ω^2 [44] (see Supplemental Material [42] for an illustration of such beating effects in harmonically trapped systems). By contrast, a spin perturbation produces a strong excitation of the spin mode (and

thus of the stripe pattern) with practically invisible beating in the stripe wave vector since the contribution of the density mode is of order Ω^4, as noted below Eq. (9).

Experimental perspectives.—For the study of stripe dynamics, it is favorable to have stripes with high contrast. This requires strong miscibility between the two components to suppress the transition to the phase-separated plane-wave phase. It is therefore best to use an atom where the scattering lengths are tunable via Feshbach resonances, such as ^{39}K [50] or ^{7}Li [51]. Alternatively, in species with low bulk miscibility, such as ^{87}Rb, the critical Raman coupling for the stripe phase can be enhanced by considering a quasi-2D configuration characterized by a reduced spatial overlap of the two spin components in the strongly confined direction. This can be realized experimentally with the help of a spin-dependent trapping potential [45,52,53] (as we have assumed in our numerics above) or using pseudospin orbital states in a superlattice [9].

The stripe pattern for SOC BECs has been observed via Bragg scattering [9,10]. Since the Bragg angle depends on the period (and angle) of the stripes, any oscillation in the stripe spacing (or orientation) will result in an oscillating Bragg signal. Our simulations for realistic parameters show a modulation of the stripe wave vector on the order of 5%. This should be easily resolvable in experiments since the angular resolution of the Bragg spot is diffraction limited by the condensate size, which is typically 10 to 50 times larger than the fringe spacing. Alternatively, the periodic dilatation or rotation of the stripe wave vector could be observed by identifying the oscillating peaks in the momentum distribution after ballistic expansion. The dynamics of the stripes, including their zero-frequency translational motion, may also be observed *in situ* after increasing the stripe period to several microns, e.g., by creating a spatial beat note with the pattern imprinted by a $\pi/2$ Raman pulse [45] or by using matter-wave-lensing techniques [54,55]. Interestingly, since the phase of the Raman beams is added to the spontaneous phase due to symmetry breaking, an oscillation of the position of the stripes can be driven by a frequency detuning of the Raman beams and could possibly be detected by an increase in temperature after dissipative damping.

In conclusion, SOC supersolids display a rich dynamics of their spontaneously established crystal order. This is similar to the dynamics predicted and observed in dipolar quantum gases [15–17]. The main difference between the two systems is that SOC supersolids have a spin degree of freedom, which provides a natural way to excite the crystal Goldstone mode. This supersolid Goldstone mode is of hybridized spin-density nature. Its dynamics is different from that of supersolids mediated by two single-mode cavities, where nonzero wave vectors are suppressed by the infinite-range coupling [11,31], and in strong distinction from externally imposed rigid density patterns as in optical lattices. As we have shown, the predicted dynamics in SOC supersolids is readily accessible within state-of-the-art experimental capabilities.

This project has received funding from the European Research Council (ERC) under the European Union's Horizon 2020 research and innovation programme (Grant Agreement No. 804305). This work has been supported by Q@TN, the joint lab between the University of Trento, FBK—Fondazione Bruno Kessler, INFN—National Institute for Nuclear Physics, and CNR—National Research Council. We further acknowledge support by Provincia Autonoma di Trento, from the Italian Ministry of University and Research (MUR) through the PRIN project INPhoPOL (Grant No. 2017P9FJBS) and the PNRR MUR Project No. PE0000023—NQSTI, and from the National Science Foundation through the Center for Ultracold Atoms and Grant No. 1506369.

K. T. G. and G. I. M. contributed equally to this work.

*kevinthomas.geier@unitn.it
†giovanni_italo.martone@lkb.upmc.fr

[1] E. P. Gross, Unified theory of interacting bosons, Phys. Rev. **106**, 161 (1957).
[2] E. P. Gross, Classical theory of boson wave fields, Ann. Phys. (N.Y.) **4**, 57 (1958).
[3] D. J. Thouless, The flow of a dense superfluid, Ann. Phys. (N.Y.) **52**, 403 (1969).
[4] A. F. Andreev and I. M. Lifshitz, Quantum theory of defects in crystals, Zh. Eksp. Teor. Fiz. **56**, 2057 (1969) [Sov. Phys. JETP **29**, 1107 (1969)].
[5] A. J. Leggett, Can a Solid be Superfluid?, Phys. Rev. Lett. **25**, 1543 (1970).
[6] D. A. Kirzhnits and Y. A. Nepomnyashchii, Coherent crystallization of quantum liquid, Zh. Eksp. Teor. Fiz. **59**, 2203 (1970) [Sov. Phys. JETP **32**, 1191 (1971)].
[7] S. Balibar, The enigma of supersolidity, Nature (London) **464**, 176 (2010).
[8] M. Boninsegni and N. V. Prokof'ev, Colloquium: Supersolids: What and where are they?, Rev. Mod. Phys. **84**, 759 (2012).
[9] J.-R. Li, J. Lee, W. Huang, S. Burchesky, B. Shteynas, F. Ç. Top, A. O. Jamison, and W. Ketterle, A stripe phase with supersolid properties in spin-orbit-coupled Bose-Einstein condensates, Nature (London) **543**, 91 (2017).
[10] A. Putra, F. Salces-Cárcoba, Y. Yue, S. Sugawa, and I. B. Spielman, Spatial Coherence of Spin-Orbit-Coupled Bose Gases, Phys. Rev. Lett. **124**, 053605 (2020).
[11] J. Léonard, A. Morales, P. Zupancic, T. Esslinger, and T. Donner, Supersolid formation in a quantum gas breaking a continuous translational symmetry, Nature (London) **543**, 87 (2017).
[12] L. Tanzi, E. Lucioni, F. Famà, J. Catani, A. Fioretti, C. Gabbanini, R. N. Bisset, L. Santos, and G. Modugno, Observation of a Dipolar Quantum Gas with Metastable Supersolid Properties, Phys. Rev. Lett. **122**, 130405 (2019).

[13] F. Böttcher, J.-N. Schmidt, M. Wenzel, J. Hertkorn, M. Guo, T. Langen, and T. Pfau, Transient Supersolid Properties in an Array of Dipolar Quantum Droplets, Phys. Rev. X **9**, 011051 (2019).
[14] L. Chomaz, D. Petter, P. Ilzhöfer, G. Natale, A. Trautmann, C. Politi, G. Durastante, R. M. W. van Bijnen, A. Patscheider, M. Sohmen, M. J. Mark, and F. Ferlaino, Long-lived and Transient Supersolid Behaviors in Dipolar Quantum Gases, Phys. Rev. X **9**, 021012 (2019).
[15] L. Tanzi, S. M. Roccuzzo, E. Lucioni, F. Famà, A. Fioretti, C. Gabbanini, G. Modugno, A. Recati, and S. Stringari, Supersolid symmetry breaking from compressional oscillations in a dipolar quantum gas, Nature (London) **574**, 382 (2019).
[16] M. Guo, F. Böttcher, J. Hertkorn, J.-N. Schmidt, M. Wenzel, H. P. Büchler, T. Langen, and T. Pfau, The low-energy Goldstone mode in a trapped dipolar supersolid, Nature (London) **574**, 386 (2019).
[17] G. Natale, R. M. W. van Bijnen, A. Patscheider, D. Petter, M. J. Mark, L. Chomaz, and F. Ferlaino, Excitation Spectrum of a Trapped Dipolar Supersolid and its Experimental Evidence, Phys. Rev. Lett. **123**, 050402 (2019).
[18] D. Petter, A. Patscheider, G. Natale, M. J. Mark, M. A. Baranov, R. van Bijnen, S. M. Roccuzzo, A. Recati, B. Blakie, D. Baillie, L. Chomaz, and F. Ferlaino, Bragg scattering of an ultracold dipolar gas across the phase transition from Bose-Einstein condensate to supersolid in the free-particle regime, Phys. Rev. A **104**, L011302 (2021).
[19] L. Chomaz, I. Ferrier-Barbut, F. Ferlaino, B. Laburthe-Tolra, B. L. Lev, and T. Pfau, Dipolar physics: A review of experiments with magnetic quantum gases, Rep. Prog. Phys. **86**, 026401 (2023).
[20] Y.-J. Lin, R. L. Compton, K. Jiménez-García, J. V. Porto, and I. B. Spielman, Synthetic magnetic fields for ultracold neutral atoms, Nature (London) **462**, 628 (2009).
[21] Y.-J. Lin, K. Jiménez-García, and I. B. Spielman, Spin-orbit-coupled Bose-Einstein condensates, Nature (London) **471**, 83 (2011).
[22] C. Wang, C. Gao, C.-M. Jian, and H. Zhai, Spin-Orbit-Coupled Spinor Bose-Einstein Condensates, Phys. Rev. Lett. **105**, 160403 (2010).
[23] T.-L. Ho and S. Zhang, Bose-Einstein Condensates with Spin-Orbit Interaction, Phys. Rev. Lett. **107**, 150403 (2011).
[24] C.-J. Wu, I. Mondragon-Shem, and X.-F. Zhou, Unconventional Bose-Einstein condensations from spin-orbit coupling, Chin. Phys. Lett. **28**, 097102 (2011).
[25] Y. Li, L. P. Pitaevskii, and S. Stringari, Quantum Tricriticality and Phase Transitions in Spin-Orbit-Coupled Bose-Einstein Condensates, Phys. Rev. Lett. **108**, 225301 (2012).
[26] Y. Li, G. I. Martone, L. P. Pitaevskii, and S. Stringari, Superstripes and the Excitation Spectrum of a Spin-Orbit-Coupled Bose-Einstein Condensate, Phys. Rev. Lett. **110**, 235302 (2013).
[27] Y. Li, G. I. Martone, and S. Stringari, Spin-orbit-coupled Bose-Einstein condensates, in *Annual Review of Cold Atoms and Molecules*, edited by K. W. Madison, K. Bongs, L. D. Carr, A. M. Rey, and H. Zhai (World Scientific, Singapore, 2015), Vol. 3, Chap. 5, pp. 201–250.
[28] K. T. Geier, G. I. Martone, P. Hauke, and S. Stringari, Exciting the Goldstone Modes of a Supersolid Spin-Orbit-Coupled Bose Gas, Phys. Rev. Lett. **127**, 115301 (2021).
[29] G. I. Martone and S. Stringari, Supersolid phase of a spin-orbit-coupled Bose-Einstein condensate: A perturbation approach, SciPost Phys. **11**, 92 (2021).
[30] L. Chen, H. Pu, Z.-Q. Yu, and Y. Zhang, Collective excitation of a trapped Bose-Einstein condensate with spin-orbit coupling, Phys. Rev. A **95**, 033616 (2017).
[31] J. Léonard, A. Morales, P. Zupancic, T. Donner, and T. Esslinger, Monitoring and manipulating Higgs and Goldstone modes in a supersolid quantum gas, Science **358**, 1415 (2017).
[32] The situation is different for multi-mode cavities, see, e.g., Ref. [33].
[33] Y. Guo, R. M. Kroeze, B. P. Marsh, S. Gopalakrishnan, J. Keeling, and B. L. Lev, An optical lattice with sound, Nature (London) **599**, 211 (2021).
[34] J. Dalibard, F. Gerbier, G. Juzeliūnas, and P. Öhberg, Colloquium: Artificial gauge potentials for neutral atoms, Rev. Mod. Phys. **83**, 1523 (2011).
[35] V. Galitski and I. B. Spielman, Spin-orbit coupling in quantum gases, Nature (London) **494**, 49 (2013).
[36] M. Aidelsburger, S. Nascimbene, and N. Goldman, Artificial gauge fields in materials and engineered systems, C. R. Phys. **19**, 394 (2018).
[37] W. Zheng, Z.-Q. Yu, X. Cui, and H. Zhai, Properties of Bose gases with the Raman-induced spin-orbit coupling, J. Phys. B **46**, 134007 (2013).
[38] X.-L. Chen, J. Wang, Y. Li, X.-J. Liu, and H. Hu, Quantum depletion and superfluid density of a supersolid in Raman spin-orbit-coupled Bose gases, Phys. Rev. A **98**, 013614 (2018).
[39] L. P. Pitaevskii and S. Stringari, *Bose-Einstein Condensation and Superfluidity*, 1st ed., International Series of Monographs on Physics Vol. 164 (Oxford University Press, Oxford, United Kingdom, 2016).
[40] Note that the plane-wave phase leads to phase separation into two domains, one mainly spin up, the other mainly spin down. In each domain, the phase between spin-up and down components is locked.
[41] G. I. Martone, Y. Li, L. P. Pitaevskii, and S. Stringari, Anisotropic dynamics of a spin-orbit-coupled Bose-Einstein condensate, Phys. Rev. A **86**, 063621 (2012).
[42] See Supplemental Material at http://link.aps.org/supplemental/10.1103/PhysRevLett.130.156001, where the additional Ref. [43] has been included, for further information on the dispersion of collective excitations, the perturbation approach in infinite systems, the translational motion of stripes, and the beating effects caused by density perturbations.
[43] Y. Li, G. I. Martone, and S. Stringari, Sum rules, dipole oscillation and spin polarizability of a spin-orbit-coupled quantum gas, Europhys. Lett. **99**, 56008 (2012).
[44] G. I. Martone, Quench dynamics of a supersolid spin-orbit-coupled Bose gas: A perturbation approach (to be published).
[45] G. I. Martone, Y. Li, and S. Stringari, Approach for making visible and stable stripes in a spin-orbit-coupled Bose-Einstein superfluid, Phys. Rev. A **90**, 041604(R) (2014).

[46] J. Radić, T. A. Sedrakyan, I. B. Spielman, and V. Galitski, Vortices in spin-orbit-coupled Bose-Einstein condensates, Phys. Rev. A **84**, 063604 (2011).
[47] C. Qu and S. Stringari, Angular Momentum of a Bose-Einstein Condensate in a Synthetic Rotational Field, Phys. Rev. Lett. **120**, 183202 (2018).
[48] S. Stringari, Diffused Vorticity and Moment of Inertia of a Spin-Orbit-Coupled Bose-Einstein Condensate, Phys. Rev. Lett. **118**, 145302 (2017).
[49] Vice versa, a spin perturbation also generates a beat note in density observables.
[50] N. B. Jørgensen, L. Wacker, K. T. Skalmstang, M. M. Parish, J. Levinsen, R. S. Christensen, G. M. Bruun, and J. J. Arlt, Observation of Attractive and Repulsive Polarons in a Bose-Einstein Condensate, Phys. Rev. Lett. **117**, 055302 (2016).
[51] T. Secker, J. Amato-Grill, W. Ketterle, and S. Kokkelmans, High-precision analysis of Feshbach resonances in a Mott insulator, Phys. Rev. A **101**, 042703 (2020).
[52] G. I. Martone, Visibility and stability of superstripes in a spin-orbit-coupled Bose-Einstein condensate, Eur. Phys. J. Special Topics **224**, 553 (2015).
[53] J. de Hond, J. Xiang, W. C. Chung, E. Cruz-Colón, W. Chen, W. C. Burton, C. J. Kennedy, and W. Ketterle, Preparation of the Spin-Mott State: A Spinful Mott Insulator of Repulsively Bound Pairs, Phys. Rev. Lett. **128**, 093401 (2022).
[54] P. A. Murthy, D. Kedar, T. Lompe, M. Neidig, M. G. Ries, A. N. Wenz, G. Zürn, and S. Jochim, Matter-wave Fourier optics with a strongly interacting two-dimensional Fermi gas, Phys. Rev. A **90**, 043611 (2014).
[55] L. Tarruell (private communication).